### Title

Effects of Styrene-Maleic Acid (SMA) Copolymer on the Photoactivation Mechanism of Rhodopsin




### Journal

BIOPHYSICAL JOURNAL, 118(3)

### ISSN

0006-3495



### Authors

Pitch, Stephanie G
Szundi, Istvan
Yao, Weekie
et al.



### Publication Date

2020

Peer reviewed

Biophysical Journal
Article

Biophysical Society

# Functional integrity of membrane protein rhodopsin solubilized by styrene-maleic acid copolymer

Stephanie G. Pitch,[1] Weekie Yao,[2] Istvan Szundi,[1] Jonathan Fay,[2] Eefei Chen,[1] Anthony Shumate,[2] David S. Kliger,[1] and David L. Farrens[2,*]

[1]Department of Chemistry and Biochemistry, University of California, Santa Cruz, Santa Cruz, California and [2]Department of Chemical Physiology and Biochemistry, Oregon Health and Science University, Portland, Oregon

ABSTRACT Membrane proteins often require solubilization to study their structure or define the mechanisms underlying their function. In this study, the functional properties of the membrane protein rhodopsin in its native lipid environment were investigated after being solubilized with styrene-maleic acid (SMA) copolymer. The static absorption spectra of rhodopsin before and after the addition of SMA were recorded at room temperature to quantify the amount of membrane protein solubilized. The samples were then photobleached to analyze the functionality of rhodopsin upon solubilization. Samples with low or high SMA/rhodopsin ratios were compared to find a threshold in which the maximal amount of active rhodopsin was solubilized from membrane suspensions. Interestingly, whereas the highest SMA/rhodopsin ratios yielded the most solubilized rhodopsin, the rhodopsin produced under these conditions could not reach the active (Meta II) state upon photoactivation. The results confirm that SMA is a useful tool for membrane protein research, but SMA added in excess can interfere with the dynamics of protein activation.

SIGNIFICANCE Styrene-maleic acid (SMA) copolymers are promising tools for solubilizing and studying membrane proteins. Cell membranes can be treated with SMA to directly solubilize membrane proteins while retaining their surrounding lipids, thus potentially preserving protein conformations that might be altered using detergents. We tested how SMA affects rhodopsin, using the light-sensitive retinal chromophore to report on SMA-induced changes in receptor conformation and dynamics. The results show that a range of SMA concentrations can be used to effectively solubilize rhodopsin from native rod outer segment membranes. However, the amount of SMA that is used affects receptor function differently; at high SMA concentrations, the rhodopsin cannot undergo full light activation to the active (Meta II) state, whereas at low amounts it can.

## INTRODUCTION

Cell-surface membrane proteins play vital roles in cellular homeostasis and activity, often acting as the communication interface between the internal and external cellular environments (1,2). Information about membrane protein structure, function, and dynamics is thus critical for a basic understanding of biological processes. Acquiring such information is difficult because it is often crucial to retain the hydrophobic membrane environment around the protein to ensure its stability and functional dynamics (3–5), and the presence of these membranes and lipid components introduces experimental challenges for structural and biophysical studies.

Membrane proteins are often studied after extracting the protein from the lipid bilayer to circumvent these challenges, which is commonly achieved through the use of detergents (3). Detergents insert their hydrophobic tails into the lipidic membrane and begin to extract the protein as the concentration of detergent passes the critical micelle concentration and micelles spontaneously form (6). Unfortunately, this process also often causes the membrane proteins to become stripped of all endogenous lipids (4,5), thus potentially compromising the protein's structural and functional integrity.

G-protein-coupled receptors (GPCRs) are a particularly important group of membrane proteins. The largest family of membrane proteins in the human genome, GPCRs are used to detect a broad spectrum of extracellular signals,

*Submitted November 19, 2020, and accepted for publication May 13, 2021.*

*Correspondence: farrensd@ohsu.edu

Stephanie G. Pitch and Weekie Yao contributed equally to this work.

Jonathan Fay's present address is Department of Biochemistry and Biophysics, University of North Carolina, Chapel Hill, North Carolina.

Editor: Sudha Chakrapani.

https://doi.org/10.1016/j.bpj.2021.05.008

including photons, ions, small organic molecules, and proteins (2,7). Thus, understanding how the lipid bilayer affects their structure and function is of significant interest.

The dim light-sensitive receptor rhodopsin is one of the most studied GPCRs and the first for which a high-resolution crystal structure was determined (8). The ability of rhodopsin to sense light is due to its 11-*cis*-retinal chromophore that is covalently attached to Lys-296 in the apoprotein (opsin) through a protonated Schiff base linkage. Light induces photoisomerization of this chromophore, which then triggers a series of intermediates that ultimately result in the formation of the active-state metarhodopsin (Meta) II (7,9). Meta II then couples to the G-protein transducin to trigger an enzyme cascade, leading to visual transduction. The composition of the lipid bilayer and its influence on the photoactivation of rhodopsin have been studied for over 30 years by the laboratories of Litman and Mitchell (10,11), Brown (12,13), and, recently, by us (14).

Detergents are known to significantly impact the dynamics of membrane proteins (15,16). The ability to activate rhodopsin by light and then track the resulting dynamic changes by spectroscopy can be used to assess how detergents affect its structure, dynamics, and function. Rhodopsin early intermediates (that reflect structural changes around the chromophore) are not sensitive to detergents, whereas the dynamics of late intermediates (related to global protein structural changes for function) are quite sensitive to detergents (17). For these reasons, rhodopsin provides an excellent platform for identifying membrane protein solubilizing agents that are less harsh in affecting the lipid bilayer to study the functional properties of membrane proteins. One approach, incorporating rhodopsin into so-called nanodiscs guided by membrane scaffold proteins, has been shown to preserve activation dynamics (18). Unfortunately, the process of preparing and characterizing rhodopsin-nanodisc samples is quite experimentally involved and often requires the incorporation of non-native lipids. Thus, we decided to investigate an alternative approach that was gaining attention.

Amphipathic copolymers, such as styrene-maleic acid (SMA), show great promise as alternative solubilizing agents (4,19–21). Like detergents, the hydrophobic monomer unit inserts into the lipidic membrane to extract the protein (22,23). However, SMA can be used to solubilize active protein in such a way that the protein remains surrounded by a patch of endogenous lipids, often termed SMA lipid particles (SMALPs). SMALPs are an excellent tool for a broad range of experimental techniques, from transmission and cryogenic electron microscopy to circular dichroism (5). As this system becomes more widely used for structural studies of membrane proteins (24,25), it is important to define how the SMA-stabilized lipid environment affects the functional properties of membrane proteins. Thus, we sought to assess whether SMA affects the solubilized protein and determine whether there are conditions that retain optimal functional integrity.

In this study, we extracted native bovine rhodopsin with SMALPs (rhodopsin-SMALPs) and assessed the functionality of the solubilized product. As discussed earlier, rhodopsin provides an ideal model system to investigate the functional integrity of a membrane protein because its activation mechanism is initiated with light, and absorption spectroscopy can monitor the progression of the reaction intermediates (26). Thus, the absorption spectra of photolysis products from rhodopsin-SMALPs allowed us to judge the ability of rhodopsin to function in an SMA-stabilized lipid environment. Because absorption spectroscopy can also determine the concentration of rhodopsin in solution, we could quantify the solubilization efficiency of SMA based on the original amount of rhodopsin in the native membrane. We found that decreasing the molar ratio between SMA and rhodopsin results in less protein solubilized. However, SMA added in excess significantly affects the protein dynamics and thus the functional properties of rhodopsin.

## MATERIALS AND METHODS

### Preparation of SMA copolymer stock solution

SMA 3:1 copolymer (Polyscope Polymers BV, Geleen, the Netherlands) has a weight average molecular weight of 10 kDa (Fig. 1 *a*). SMA was precipitated by the addition of 6 M HCl, rinsed with sterile water, and collected by filtration. The SMA stock solution (5% w/v) was made by dissolving SMA powder in 50 mM Tris, 40 mM NaCl, adjusted to pH 8, then stored at −20°C. SMA copolymers aggregate at low pH (below pH 5.25 for the 3:1 SMA variant), which can be identified by an increase in the apparent optical density due to light scattering (20).

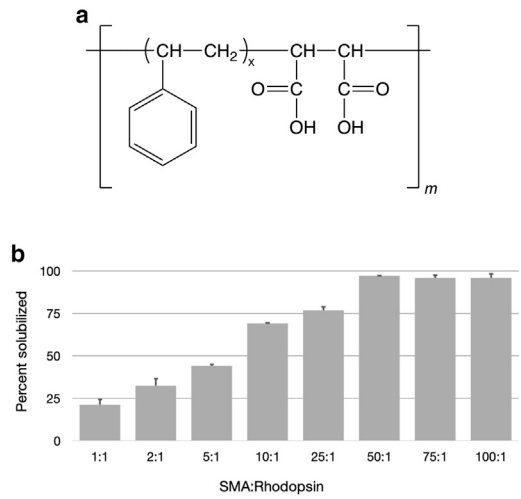


FIGURE 1 (*a*) Chemical structure of SMA. On average, m ≈ 9 and x ≈ 3 for SMA (3:1). (*b*) Solubilization efficiency of SMA as a function of the ratio of SMA units/rhodopsin units. Data are averages of two independent samples, and the positive error value represents the difference in solubilization between both samples.

### Preparation of native membrane suspension

Sample preparation was carried out under red light. Native bovine rhodopsin in disc membranes was isolated from rod outer segments (ROS) and then hypotonically washed as reported previously (27). The samples were resuspended in Tris buffer (10 mM Tris, 100 mM NaCl, pH 8). Between pH 6.0 and 8.0, we found that the 3:1 SMA variant formed the most stable rhodopsin-SMALPs at pH 8. The functions of rhodopsin at pH 8 are similar to those at neutral pH, but pH 8 shows the most rhodopsin intermediates upon photoactivation (14). For these reasons, we decided to use pH 8 for this study. The concentration of rhodopsin was determined spectrophotometrically (V750; JASCO, Easton, MD) by measuring the change in absorbance at 500 nm ($\varepsilon_{500}$ = 40,600 $M^{-1}$ $cm^{-1}$) before and after irradiation in the presence of Tris buffer. The spectral ratio of rhodopsin ($A_{280}/A_{500}$) was 2.3 for the sample in this study.

### Formation of rhodopsin-SMALPs

Samples with molar ratios between 1 and 100 SMA per rhodopsin were prepared by adding appropriate amounts of 5% (w/v) SMA stock solution to aliquots of native membrane suspensions containing ~0.2 mg of rhodopsin (200 $\mu$L of 1 mg/mL). Tris buffer was added to bring the samples to the same volume, and after mixing, the samples were centrifuged at 10,000 $\times$ $g$ for 20 min at 4°C. The soluble fraction that contained rhodopsin-SMALPs was collected for further analysis, and the pellet was discarded.

### Static photobleaching measurements

Rhodopsin-SMALPs were characterized spectrophotometrically in the 250–700 nm wavelength range at room temperature. The solubilization efficiency of SMA was quantified by measuring the absorption spectra of the soluble fractions and comparing those with the spectra collected before centrifugation. The second set of spectra were recorded after irradiating the samples for 30 s to characterize the functional properties of solubilized rhodopsin. The light source used to irradiate the samples was a tungsten-halogen lamp (150 W) that was 6 inches away from the sample holder, and a yellow filter was placed in front of the sample. For the SMA/rhodopsin molar ratio of 50, the time dependence of absorption changes post-photolysis was recorded at 15-min intervals for a total of 45 min.

### Retinal release assay

The release of retinal from photoactivated rhodopsin was monitored by measuring the increase in opsin tryptophan (Trp) fluorescence using a PTI QuantaMaster Series-1 (Photon Technology International, Birmingham, NJ) spectrophotometer. Fluorescence measurements were started on samples in the dark. The rhodopsin samples (0.5 $\mu$M) were activated with $\lambda > 495$-nm light for 30 s, and the subsequent increase in fluorescence was monitored over time. Measurements were at ~24°C, with emission monitored at 330 nm and excitation provided by a 295 nm LED (LLS-295; Ocean Optics, Dunedin, FL). SMA-solubilized rhodopsin samples (25:1 and 100:1 molar ratios) were prepared as described earlier. To prepare the rhodopsin samples solubilized with $n$-dodecyl-$\beta$-D-maltoside (DDM), ROS was solubilized with 1% DDM in the dark at 4°C for 30 min, clarified at 10,000 $\times$ $g$ for 20 min, then diluted to 0.05% DDM in SMA buffer before use. The Trp fluorescence of dark-state rhodopsin and buffer ($F_0$) was subtracted from total Trp fluorescence (F). Data were fitted to $F(t) = C + A(1-e^{-bt})$ for DDM-solubilized rhodopsin, and $F(t) = C + A(1 - e^{-bt}) + D(1 - e^{-gt})$ for SMA-solubilized rhodopsin, using the "curve_fit" function in SciPy Python package.

### $NaBH_4$ reduction

SMA (25:1 and 100:1 molar ratios with rhodopsin) and DDM-solubilized ROS membranes (0.05% DDM) were prepared as described earlier. For each experimental data point, 20 $\mu$L of 3 $\mu$M rhodopsin was photoactivated with $\lambda > 495$ nm light for 30 s, then allowed to decay at room temperature in the dark for either 30 or 120 min. Afterward, 5 $\mu$L of 1% $NaBH_4$ (freshly prepared in 20$\times$ PBSSC (0.137 M NaCl, 2.7 mM KCl, 1.5 mM KH2PO4, and 8 mM Na2HPO4, pH 7.2)) was added to reduce any retinal Schiff base present. The "0 min" time point (t = 0) was obtained by adding $NaBH_4$ to the sample before light irradiation.

After the addition of $NaBH_4$, samples were incubated on ice in the dark for 10 min, then subjected to SDS-PAGE analysis followed by imaging to detect $n$-retinylidene opsin fluorescence using an Alpha Innotech FluorChem 5500 (Alpha Innotech, San Leandro, CA) imager (365-nm excitation, emission detected for 8 s through the instrument's SYBR Green filter). The resulting fluorescent gel images were processed in Adobe Photoshop (using "Auto Contrast"), and the intensity of the band was inverted for comparison with the subsequent Coomassie-stained gel. The fluorescence intensities of each band were quantified using ImageJ software.

## RESULTS

### Solubilization efficiency is dependent on the SMA/rhodopsin ratio

The concentration of the solubilizing agent SMA and the amounts of proteins and lipids in the membranes are the main factors that influence solubilization efficiency from native bovine ROS disc membranes. In the solubilization experiment, we kept the rhodopsin concentration constant. Because the membrane contains rhodopsin and lipids in a fixed ratio, the mass of membrane subject to solubilization was the same in the samples, leaving SMA concentration as the variable parameter. SMA concentrations were chosen to provide SMA/rhodopsin molar ratios of 1, 2, 5, 10, 25, 50, 75, and 100. Rhodopsin can be recovered in the solubilized fraction after centrifugation of the membrane suspension. We determined the percentage of solubilized protein from the ratio of absorbance values at 500 nm for the sample before and after centrifugation. As displayed in Fig. 1 *b*, the fraction of solubilized rhodopsin increased as the SMA/rhodopsin ratio increased up to a value of 50. Above this ratio, percentage solubilizations are very similar at ~95%.

### Characterization of the rhodopsin-SMALPs

After photoexcitation, rhodopsin undergoes a sequence of transitions through several intermediates before it reaches the active state. It is believed that the deprotonated intermediate Meta II ($\lambda_{max}$ = 380 nm) is the active form capable of binding the G-protein. Meta II is in equilibrium with the protonated intermediate Meta $I_{480}$ ($\lambda_{max}$ = 480 nm) and differs from it not only by the protonation state of the Schiff base but also by the relative arrangement of the transmembrane helices. At room temperature, the active state of rhodopsin in native membrane is reached in 10–20 ms after excitation (28). It is then stable for at least a couple of

minutes before it decays to a complex mixture of different forms commonly referred to as Meta III.

Thus, in photobleaching experiments on native membranes, the spectra of the photoproducts recorded on the minute timescale are often used to characterize the active state of rhodopsin. Because the equilibrium between Meta $I_{480}$ and Meta II is sensitive to the lipid environment of the rhodopsin molecule, we use spectra recorded at roughly 1 min after illumination to test whether rhodopsin reaches the active state in SMALPs. After measuring the absorption spectra of rhodopsin-SMALPs in the dark, the samples were irradiated for 30 s, and absorption spectra of the photoproducts were recorded.

In addition to rhodopsin absorption, the spectra recorded are complicated by light scattering and by the absorbance due to SMA in the solubilized samples, which is the dominant component in the 250–300 nm ultraviolet region at high SMA/rhodopsin ratios. Each recorded spectrum was corrected for SMA and light scattering contributions by subtracting an appropriately scaled SMA spectrum and a scattering function. We applied a combination of the light scattering functions known for molecules and small particles (the Rayleigh scattering), $\sim\lambda^{-4}$, and the approximation applicable to big particles, $\sim\lambda^{-2}$, for the membrane and the samples before centrifugation. For the solubilized samples post-centrifugation shown in Fig. 2, only the $\sim\lambda^{-4}$ function was required to produce the corrected spectra. This approach allowed us to quantitatively analyze the spectral forms of rhodopsin that were present after bleaching.

Below 300 nm, the corrected spectra have limited accuracy because of distortions in recording SMA absorbance, particularly for the samples with high SMA/rhodopsin ratios. Thus, the 280-nm protein absorption band in the corrected spectra is not accurate enough to draw definite conclusions regarding the effect of SMA on this band or the 280/500 absorption ratio. The corrected absorption spectra of the samples taken prephotolysis, normalized to 1 at 500 nm, are shown in Fig. 3 *a*. The spectra for all SMA/rhodopsin ratios overlap and are hard to distinguish except in the 280-nm region. The amplitude of the 280-nm band is roughly twice that of the 500-nm visible band, which suggests that the protein is most likely fairly intact. Only samples with very high SMA/rhodopsin ratios might deviate slightly. However, we cannot draw firm conclusions based on the small differences seen in the figure.

Spectra taken post-photolysis were corrected and normalized in a similar way, using practically the same SMA absorption and light scattering values and the same normalization factors that were used for the spectra taken prephotolysis. The normalized spectra are shown in Fig. 3 *b*. For samples with SMA/rhodopsin ratios of 1, 2, 5, and 10, the spectra of the photoproducts are consistent with an active state formed by the Meta II and Meta $I_{480}$ intermediates and having Meta $I_{480}$ fraction values of 0.26, 0.3, 0.32, and 0.33, respectively. Considering that the absorption spectra recorded for the lowest ratios had small amplitudes and thus were less accurate, these fraction values represent practically the same Meta $I_{480}$ content in the

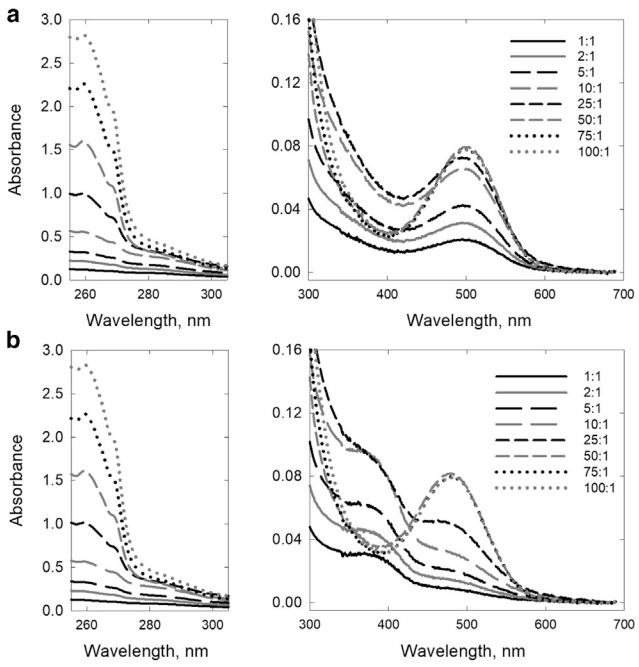


FIGURE 2 Absorbance spectra of rhodopsin-SMALPs recorded (*a*) pre- and (*b*) post-photolysis for SMA/rhodopsin molar ratios from 1 (smallest) to 100 (biggest).

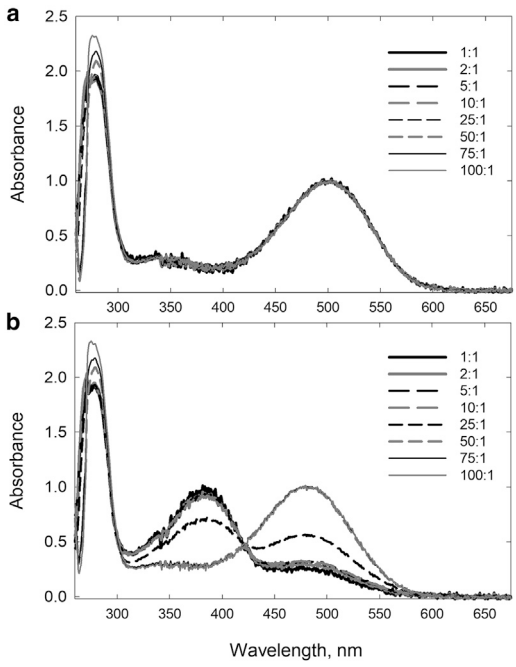


FIGURE 3 Absorbance spectra (*a*) pre- and (*b*) post-photolysis displayed in Fig. 2 after being corrected for SMA and scattering contributions and normalized to 1 A.U. at 500 nm.

photoproducts. For the SMA/rhodopsin ratio of 25, the Meta $I_{480}$ component is significantly higher, with a fraction value of 0.55. Interestingly, for ratios of 50, 75, and 100, the Meta $I_{480}$ form is the only photoproduct. Meta $I_{480}$ is expected to become the dominant or only photoproduct recorded if the 1-min delay time after illumination is too short to reach the final equilibrium between Meta $I_{480}$ and Meta II. Alternatively, the equilibrium may be back-shifted to favor Meta $I_{480}$ at high SMA/rhodopsin ratios.

To test which one of the earlier alternative explanations is more likely, we studied the sample with SMA/rhodopsin molar ratio of 50 further. The recording time post-photolysis was extended to 45 min with 15-min intervals. The results are shown in Fig. 4. There is no noticeable shift in the equilibrium toward Meta II on longer timescales. Instead, the Meta $I_{480}$ present at 1 min post-photolysis gradually converts into products that appear somewhat blue-shifted from 480 nm. This important observation indicates that the reason for observing Meta $I_{480}$ as the only product at 1 min after illumination is "not" due to a slowed-down equilibration between Meta $I_{480}$ and Meta II. Rather, it is the consequence of the equilibrium being heavily back-shifted toward Meta $I_{480}$, with practically no Meta II present.

We also tested whether the high SMA concentrations altered the release of retinal from rhodopsin using two different approaches (Fig. 5). First, we monitored increases in rhodopsin tryptophan fluorescence after photoactivation, in which changes reflect the release of retinal from the receptor binding pocket (29). Experiments were carried out with SMA/rhodopsin molar ratios of 25:1 and 100:1 and compared them with DDM-solubilized rhodopsin. The higher SMA/rhodopsin ratios exhibited slower apparent retinal release rates (2.6 E−3 $s^{-1}$ for DDM; 4.0 E−3 and 0.5 E−3 $s^{-1}$ for 25:1; and 2.7 E−3 and 0.16 E−3 $s^{-1}$ for 100:1). They also showed less overall retinal release, as suggested by the lower amount of total tryptophan fluorescence (Fig. 5 *a*). However, these results can only be compared and interpreted with caution because of the differences in both light absorbance and scattering at the 295-nm excitation wavelength used in the measurements (see Fig. 2).

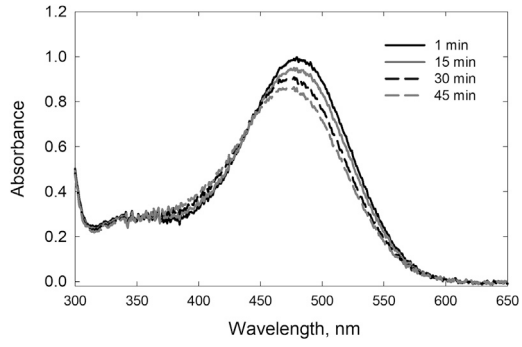


FIGURE 4 Absorbance spectra at 1, 15, 30, and 45 min post-photolysis for SMA/rhodopsin molar ratio 50. Note that for the first curve, ~1 min matches Meta $I_{480}$.

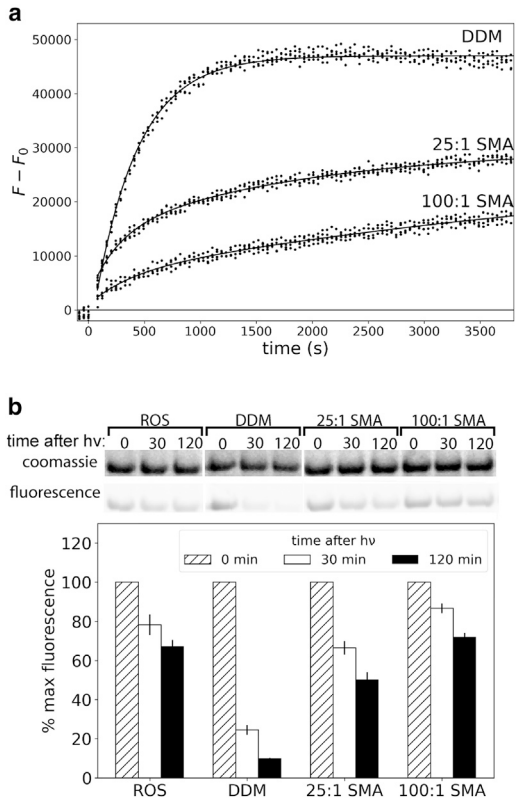


FIGURE 5 Effect of high SMA concentrations on retinal release from photobleached rhodopsin. (*a*) Tryptophan (Trp) fluorescence assay of SMA-solubilized rhodopsin (25:1 and 100:1 molar ratios) suggests slowed and reduced retinal release compared with DDM-solubilized rhodopsin. (*b*) Relative amount of Schiff base-linked retinal remaining after photobleaching determined by $NaBH_4$ reduction followed by SDS-PAGE and fluorescent imaging of rhodopsin in ROS, SMA, or DDM. The top panel shows the Coomassie-stained gels and the in-gel fluorescence. The bottom panel is a plot of the average quantified fluorescence from five independent experiments normalized to the fluorescence at t = 0. Error bars represent the standard error. Experimental details are provided in the Materials and methods.

Thus, we also quantified the amount of retinal Schiff base linkages remaining in photobleached rhodopsin using $NaBH_4$ reduction, followed by SDS-PAGE analysis and imaging to detect any fluorescent covalent retinal adducts (30). For these experiments, rhodopsin (3 $\mu$M) was solubilized in DDM or SMA, photoactivated, allowed to decay at room temperature in the dark, then reduced with $NaBH_4$ (1%) after 30 or 120 min, then subjected to SDS-PAGE and compared with control experiments in which $NaBH_4$ was added before photoactivation. The data indicate that more retinal Schiff base linkages remain in light-activated rhodopsin solubilized with a higher amount of SMA (100:1 vs. 25:1 SMA/rhodopsin) compared with DDM-solubilized rhodopsin (Fig. 5 *b*). Taken together, the retinal release and $NaBH_4$ reduction experiments suggest the retinal remains "trapped" inside photobleached rhodopsin solubilized in high amounts of SMA.

## DISCUSSION

Structural studies showed that SMALPs made by solubilization of dimyristoylphosphatidylcholine (DMPC) lipid vesicles with SMA 2:1 copolymer are disc-shaped nanoparticles having a lipid bilayer core of roughly a 7.6-nm diameter and 4.6-nm thickness. It is encircled by a 0.9-nm-thick single layer SMA belt, which shields the 2.6-nm-thick hydrophobic region of the lipid bilayer (31). Most likely, the hydrophobic styrene blocks of the copolymer form the inner layer of the belt and thus face the hydrophobic chains in the lipid core, whereas the hydrophilic maleic acid in the mixed segments are in the outer layer of the belt and interact with the surrounding water molecules and the lipid headgroups. The width of the SMA belt should match the thickness of the bilayer. Assuming a density of 1.1 g/cm$^3$, the lipid core is equivalent to a single molecule having 130–140-kDa molecular mass and the SMA belt, matching the thickness of the bilayer, to a molecule of 60–70 kDa. With an average molecular mass of 10 kDa, the SMA belt would be built by six to seven molecules. The number of SMA molecules in the belt we estimated here for DMPC, a relatively short-chain lipid, may be somewhat higher for the bilayer surrounding rhodopsin in the native membrane.

The disc membranes isolated from the ROS contain almost exclusively a single protein, rhodopsin, with a molecular mass of 40 kDa. The average number of lipid molecules per rhodopsin in the native membrane is around 70 (32,33). One rhodopsin molecule surrounded by 70 lipid molecules is equivalent to a single molecule with a 100 to 110-kDa mass. This value is very similar to the mass of the lipid core of SMALP discussed earlier. Thus, rhodopsin, with its surrounding lipids, is optimally prefabricated for solubilization by SMA, and the nanoparticles are likely to contain a single protein surrounded by its natural lipids. According to crystallographic studies, rhodopsin occupies a space equivalent to an ellipsoid with a 7.5-nm-long axis perpendicular to the membrane plane and two short axes of 4.8 and 3.5 nm in the membrane plane (9). The estimated hydrophobic portion of the molecule is equivalent to a 4.1-nm-tall cylinder, which is shielded by the unusually long fatty acyl chains of the unsaturated lipids present in the membrane (34). Thus, the lipid bilayer that surrounds rhodopsin is much thicker than 4.6 nm mentioned earlier for the DMPC lipid particle. Assuming a 6-nm-thick bilayer, the number of SMA molecules in the belt would be around 9–11. This estimate gives a roughly 1:1 mass ratio between membrane and SMA in the solubilized nanoparticle, which is in agreement with the 1:1.25 mass ratio reportedly needed for complete solubilization of POPC/POPG lipid vesicles (35). The experimental data presented here suggest that this idealistic picture of the rhodopsin-SMALP nanoparticle, deduced from the known structural information on the lipid particle, however, may not be realized at all SMA/rhodopsin ratios.

### Optimal SMA/protein solubilization ratio

Using rhodopsin as a tool to investigate solubilization by SMA has two advantages. Because the disc membrane of rod cells contains rhodopsin almost exclusively, we can monitor the amount of solubilized protein by measuring the absorbance of the sample before and after separating the SMA-solubilized fraction from the membrane suspension. Additionally, we are able to characterize the functional state of the solubilized protein and compare that with the one observed in the native membrane by photolyzing the samples and analyzing the absorption spectra of the photoproducts. The highest yield of solubilization, close to 100%, is achieved at an SMA/rhodopsin ratio of 50 and above. The photoproduct at these ratios, however, is Meta $I_{480}$ alone and not the familiar equilibrated mixture of Meta $I_{480}$ and the active form Meta II, as observed in the native membrane. At a ratio of 25, we found 0.55-part Meta $I_{480}$ and 0.45-part Meta II, which indicates that the equilibrium is heavily back-shifted toward Meta $I_{480}$ at higher ratios and somewhat back-shifted at a ratio of 25. Only at ratios from 1 to 10 did we detect an equilibrated mixture similar to the one seen in the native membrane, roughly 0.3-part Meta $I_{480}$ and 0.7-part Meta II (28).

### A possible explanation for the optimal SMA/protein solubilization ratio

As noted earlier, the protein in rhodopsin-SMALPs formed with SMA/rhodopsin molar ratios of 10 and below seems to have the same functionality as in native disc membranes. However, the "yield" of solubilized rhodopsin is lower over this range. For example, the SMA/rhodopsin ratio of 10 yields ~3/4 of the maximal value found at the highest SMA/rhodopsin ratios. Lower yield means that even at ratio 10, the amount of SMA added was not sufficient to solubilize the membrane into small-sized nanoparticles. In the discussion earlier, we estimated that ~10 SMA molecules might be needed to form a nanoparticle with one rhodopsin molecule in a pool of 70 lipid molecules. Thus, a minimal SMA/rhodopsin molar ratio of 10 is necessary for the solubilization of the rhodopsin membrane, assuming that all SMA molecules end up in the nanoparticles. This assumption, or our estimate of 10, is not entirely correct because the minimal ratio needed to solubilize the membranes seems to be higher than 10. As discussed earlier, the composition of photoproducts generated at and below the minimal solubilization ratio is similar to that of rhodopsin in its native environment, suggesting that the lipid and protein arrangement in the nanoparticle is likely to mimic the average situation that exists in the native membrane.

However, at the higher SMA/rhodopsin ratios (50 and higher), the situation is drastically different. The spectral data indicate that after light activation, the photoconversion stops at the Meta $I_{480}$ stage, suggesting an altered response (and thus environment) from that observed at low SMA/rhodopsin ratios.

What could cause this difference? One possible hypothesis is that the excess SMA may start to separate the protein and the lipids into individual nanoparticles. Consistent with this idea, we noted a sudden drop in light scattering observed for samples having SMA/rhodopsin ratios of 50 and above, suggesting that the scattering volume at high ratios may only be a fraction of that present at low ratios. A smaller scattering volume is consistent with (and would be expected) if rhodopsin is stripped of its surrounding lipids and separate protein and lipid nanoparticles are formed. We stress that this is currently only a hypothesis. Whatever the ultimate explanation, it is clear that there is a range of SMA/rhodopsin ratios optimal for preserving the membrane-like environment during solubilization. Above a threshold value (10 or slightly higher in this case), the SMA-solubilized protein may lose its full functional activity. The coincidence of the optimal and minimal solubilization ratios seen here may be accidental.

## Excess SMA reduces mobility and affects the active state

The Meta $I_{480}$–Meta II transition has been studied in great detail (36) because Meta $I_{480}$ is the last intermediate with a protonated Schiff base and the transition is crucial for receptor activation. The Meta $I_{480}$ to Meta II transition is likely to involve motions of the protein helices (37,38), which requires a mobile fluid lipid environment. When the transition is hindered in digitonin-stabilized rhodopsin (39) or by lowering the temperature (36), the equilibrium becomes back-shifted, and the Meta $I_{480}$ content in the mixture increases. This shift is seen in the sample with an SMA/rhodopsin ratio of 25. When the mobility is further reduced and the lipid membrane loses its fluidity, the Meta $I_{480}$ to Meta II equilibrium becomes heavily back-shifted. It is known from low-temperature experiments, for example, that only Meta $I_{480}$ is detected from −40 to −15°C (40). Thus, the back-shifted equilibrium we observe at high SMA/rhodopsin ratios would be consistent with a situation in which the lipids are removed, and the protein is surrounded by an inflexible SMA belt.

The time-dependent absorption changes of the sample with SMA/rhodopsin ratio 50 recorded for 45 min showed practically no Meta II formation from Meta $I_{480}$. Instead, one or more photoproducts with an absorption band blue-shifted from 480 nm are formed. To identify these products, we subtracted 0.9, 0.76, and 0.67 fractions of the Meta $I_{480}$ spectrum measured at 1 min from the spectra recorded at 15, 30, and 45 min, respectively, and normalized the resulting spectra to 100%. The spectra obtained are shown in Fig. 6. Each spectrum represents a mixture of $Meta_{460}$, $Meta_{420}$, and $Meta_{380}$ forms, contributing with fraction values of 0.66, 0.27, and 0.07, respectively. These spectral forms are typical components present in the so-called Meta III intermediate (41). This finding implies that rhodopsin stabilized by excess SMA does not reach the active Meta II state.

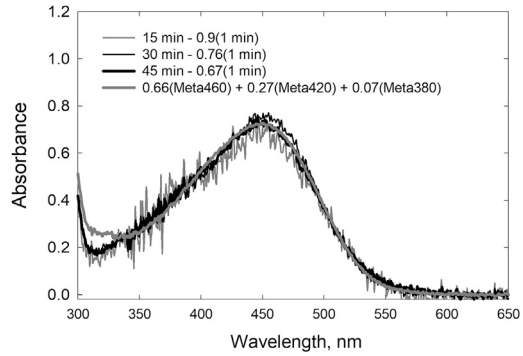


FIGURE 6 Absorption spectra of products produced in the time-dependent experiment for SMA/rhodopsin molar ratio 50. Fractions of 0.9, 0.76, and 0.67 of the 1-min spectrum were subtracted, and the resulting spectra were normalized to 100%. The heavy gray curve is composed of $0.66(Meta_{460}) + 0.27(Meta_{420}) + 0.07(Meta_{380})$.

We hypothesize that the high SMA/rhodopsin ratios may cause an increased rigidity of the protein and its surroundings that together affect photoproducts typically observed after Meta II. Although the nature of these later photoproducts was not the main focus of this study, we did test whether retinal remains attached inside the protein after photoactivation under the high SMA conditions. In contrast to photoactivated rhodopsin in DDM that converts almost exclusively to MII followed by retinal release (29), our experiments suggest the long-lasting photoproducts observed at high SMA/rhodopsin ratios contain retinal bound to a Schiff base, which is consistent with the retinal remaining inside the retinal binding pocket.

## CONCLUSIONS

As we have shown here, rhodopsin provides an excellent model system for studying how the functional properties of a membrane protein may be affected by an SMA-stabilized lipid environment. Our data show a threshold in SMA/rhodopsin ratios below which the photolyzed protein can reach the active-state composition seen in the native membrane. In contrast, above this SMA/rhodopsin ratio, the properties of the protein become different from those observed in the native membrane.

In summary, our study utilized rhodopsin to elucidate whether the solubilized protein can reach the active state. However, rhodopsin in native membrane has a complex kinetic path leading to the active state (42), and this path is highly sensitive to the lipid environment. The question of whether SMA affects the reactions and dynamics through which the active state is reached is the subject of our next study.

## ACKNOWLEDGMENTS

The authors thank Erika Reiderer and Dr. Emily Platt for their initial work on the effects of styrene-maleic acid-solubilizing native rod outer segments rhodopsin.

This work was supported by National Institutes of Health grants R01EY029343 (to D.S.K. and D.L.F.), R21DA043001 (to D.L.F.), and F31DA049438 (to A.S.).

## REFERENCES


1. Denisov, I. G., and S. G. Sligar. 2016. Nanodiscs for structural and functional studies of membrane proteins. *Nat. Struct. Mol. Biol.* 23:481–486.
2. Venkatakrishnan, A. J., X. Deupi, …, M. M. Babu. 2013. Molecular signatures of G-protein-coupled receptors. *Nature.* 494:185–194.
3. Stetsenko, A., and A. Guskov. 2017. An overview of the top ten detergents used for membrane protein crystallization. *Crystals (Basel).* 7:197.
4. Wheatley, M., J. Charlton, …, D. R. Poyner. 2016. GPCR-styrene maleic acid lipid particles (GPCR-SMALPs): their nature and potential. *Biochem. Soc. Trans.* 44:619–623.
5. Skrzypek, R., S. Iqbal, and R. Callaghan. 2018. Methods of reconstitution to investigate membrane protein function. *Methods.* 147:126–141.
6. Moraes, I., G. Evans, …, P. D. S. Stewart. 2014. Membrane protein structure determination - the next generation. *Biochim. Biophys. Acta.* 1838:78–87.
7. Smith, S. O. 2010. Structure and activation of the visual pigment rhodopsin. *Annu. Rev. Biophys.* 39:309–328.
8. Palczewski, K., T. Kumasaka, …, M. Miyano. 2000. Crystal structure of rhodopsin: a G protein-coupled receptor. *Science.* 289:739–745.
9. Palczewski, K. 2006. G protein-coupled receptor rhodopsin. *Annu. Rev. Biochem.* 75:743–767.
10. Litman, B. J., and D. C. Mitchell. 1996. A role for phospholipid polyunsaturation in modulating membrane protein function. *Lipids.* 31 (*Suppl*):S193–S197.
11. Litman, B. J., S. L. Niu, …, D. C. Mitchell. 2001. The role of docosahexaenoic acid containing phospholipids in modulating G protein-coupled signaling pathways: visual transduction. *J. Mol. Neurosci.* 16:237–242; discussion 279–284.
12. Wiedmann, T. S., R. D. Pates, …, M. F. Brown. 1988. Lipid-protein interactions mediate the photochemical function of rhodopsin. *Biochemistry.* 27:6469–6474.
13. Botelho, A. V., T. Huber, …, M. F. Brown. 2006. Curvature and hydrophobic forces drive oligomerization and modulate activity of rhodopsin in membranes. *Biophys. J.* 91:4464–4477.
14. Funatogawa, C., I. Szundi, and D. S. Kliger. 2016. A comparison between the photoactivation kinetics of human and bovine rhodopsins. *Biochemistry.* 55:7005–7013.
15. Alvarez, F. J. D., C. Orelle, …, A. L. Davidson. 2015. Full engagement of liganded maltose-binding protein stabilizes a semi-open ATP-binding cassette dimer in the maltose transporter. *Mol. Microbiol.* 98:878–894.
16. Ganapathy, S., L. Opdam, …, W. J. de Grip. 2020. Membrane matters: the impact of a nanodisc-bilayer or a detergent microenvironment on the properties of two eubacterial rhodopsins. *Biochim. Biophys. Acta Biomembr.* 1862:183113.
17. Epps, J., J. W. Lewis, …, D. S. Kliger. 2006. Lumi I–> Lumi II: the last detergent independent process in rhodopsin photoexcitationt. *Photochem. Photobiol.* 82:1436–1441.
18. Tsukamoto, H., I. Szundi, …, D. S. Kliger. 2011. Rhodopsin in nanodiscs has native membrane-like photointermediates. *Biochemistry.* 50:5086–5091.
19. Long, A. R., C. C. O'Brien, …, N. N. Alder. 2013. A detergent-free strategy for the reconstitution of active enzyme complexes from native biological membranes into nanoscale discs. *BMC Biotechnol.* 13:41.
20. Scheidelaar, S., M. C. Koorengevel, …, J. A. Killian. 2016. Effect of polymer composition and pH on membrane solubilization by styrene-maleic acid copolymers. *Biophys. J.* 111:1974–1986.
21. Voskoboynikova, N., W. Mosslehy, …, H.-J. Steinhoff. 2017. Characterization of an archaeal photoreceptor/transducer complex from Natronomonas pharaonis assembled within styrene–maleic acid lipid particles. *RSC Advances.* 7:51324–51334.
22. Dörr, J. M., S. Scheidelaar, …, J. A. Killian. 2016. The styrene-maleic acid copolymer: a versatile tool in membrane research. *Eur. Biophys. J.* 45:3–21.
23. Lee, S. C., T. J. Knowles, …, T. R. Dafforn. 2016. A method for detergent-free isolation of membrane proteins in their local lipid environment. *Nat. Protoc.* 11:1149–1162.
24. Broecker, J., B. T. Eger, and O. P. Ernst. 2017. Crystallogenesis of membrane proteins mediated by polymer-bounded lipid nanodiscs. *Structure.* 25:384–392.
25. Overduin, M., and M. Esmaili. 2019. Structures and interactions of transmembrane targets in native nanodiscs. *SLAS Discov.* 24:943–952.
26. Lewis, J. W., and D. S. Kliger. 2000. Absorption spectroscopy in studies of visual pigments: spectral and kinetic characterization of intermediates. *Methods Enzymol.* 315:164–178.
27. Thorgeirsson, T. E., J. W. Lewis, …, D. S. Kliger. 1992. Photolysis of rhodopsin results in deprotonation of its retinal Schiff's base prior to formation of metarhodopsin II. *Photochem. Photobiol.* 56:1135–1144.
28. Thorgeirsson, T. E., J. W. Lewis, …, D. S. Kliger. 1993. Effects of temperature on rhodopsin photointermediates from lumirhodopsin to metarhodopsin II. *Biochemistry.* 32:13861–13872.
29. Farrens, D. L., and H. G. Khorana. 1995. Structure and function in rhodopsin. Measurement of the rate of metarhodopsin II decay by fluorescence spectroscopy. *J. Biol. Chem.* 270:5073–5076.
30. Sommer, M. E., and D. L. Farrens. 2006. Arrestin can act as a regulator of rhodopsin photochemistry. *Vision Res.* 46:4532–4546.
31. Jamshad, M., V. Grimard, …, T. R. Dafforn. 2015. Structural analysis of a nanoparticle containing a lipid bilayer used for detergent-free extraction of membrane proteins. *Nano Res.* 8:774–789.
32. Jastrzebska, B., A. Debinski, …, K. Palczewski. 2011. Role of membrane integrity on G protein-coupled receptors: rhodopsin stability and function. *Prog. Lipid Res.* 50:267–277.
33. Soubias, O., and K. Gawrisch. 2012. The role of the lipid matrix for structure and function of the GPCR rhodopsin. *Biochim. Biophys. Acta.* 1818:234–240.
34. Teller, D. C., T. Okada, …, R. E. Stenkamp. 2001. Advances in determination of a high-resolution three-dimensional structure of rhodopsin, a model of G-protein-coupled receptors (GPCRs). *Biochemistry.* 40:7761–7772.
35. Zhang, R., I. D. Sahu, …, G. A. Lorigan. 2015. Characterizing the structure of lipodisq nanoparticles for membrane protein spectroscopic studies. *Biochim. Biophys. Acta.* 1848:329–333.
36. Matthews, R. G., R. Hubbard, …, G. Wald. 1963. Tautomeric forms of metarhodopsin. *J. Gen. Physiol.* 47:215–240.
37. Farrens, D. L., C. Altenbach, …, H. G. Khorana. 1996. Requirement of rigid-body motion of transmembrane helices for light activation of rhodopsin. *Science.* 274:768–770.
38. Ahuja, S., V. Hornak, …, M. Eilers. 2009. Helix movement is coupled to displacement of the second extracellular loop in rhodopsin activation. *Nat. Struct. Mol. Biol.* 16:168–175.
39. Szundi, I., J. W. Lewis, and D. S. Kliger. 2005. Effect of digitonin on the rhodopsin meta I-meta II equilibrium. *Photochem. Photobiol.* 81:866–873.
40. Yoshizawa, T., and G. Wald. 1963. Pre-lumirhodopsin and the bleaching of visual pigments. *Nature.* 197:1279–1286.
41. Szundi, I., J. W. Lewis, …, D. S. Kliger. 2000. Effect of NADPH on formation and decay of human metarhodopsin III at physiological temperatures. *Vision Res.* 40:3039–3048.
42. Szundi, I., C. Funatogawa, and D. S. Kliger. 2016. Complexity of bovine rhodopsin activation revealed at low temperature and alkaline pH. *Biochemistry.* 55:5095–5105.